Bloch-point-mediated topological transformations of magnetic domain walls in cylindrical nanowires

A. Wartelle,[1,*] B. Trapp,[1] M. Staňo,[1,†] C. Thirion,[1] S. Bochmann,[2] J. Bachmann,[2,3] M. Foerster,[4] L. Aballe,[4] T. O. Menteş,[5] A. Locatelli,[5] A. Sala,[5] L. Cagnon,[1] J.-C. Toussaint,[1] and O. Fruchart[6,‡]

[1]*Univ. Grenoble Alpes, CNRS, Institut Néel, F-38000 Grenoble, France*

[2]*Friedrich-Alexander Universität Erlangen-Nürnberg, Erlangen 91058, Germany*

[3]*Institute of Chemistry, Saint-Petersburg State University, Universitetskii pr. 26, 198504 St. Petersburg, Russia*

[4]*Alba Synchrotron Light Facility, CELLS, E-08290 Barcelona, Spain*

[5]*Elettra-Sincrotrone Trieste, S.C.p.A., Trieste I-34012, Italy*

[6]*Univ. Grenoble Alpes, CNRS, CEA, INAC-Spintec, F-38000 Grenoble, France*

(Received 28 June 2018; revised manuscript received 8 January 2019; published 29 January 2019)

Cylindrical nanowires made of soft magnetic materials, in contrast to thin strips, host domain walls of two distinct topologies. Following 15 years of theoretical predictions of the unique dynamic features of such walls, such as absence of Walker breakdown, we report on experiments here. Unexpectedly, we evidence the dynamic transformation of topology upon wall motion above a field threshold, a phenomenon that had been previously overlooked. Micromagnetic simulations highlight the underlying phenomenon for one type of transformation, involving the nucleation of a Bloch-point singularity. This calls for reexamining existing predictions, and further experiments to highlight the conditions favoring the transformation.

DOI: 10.1103/PhysRevB.99.024433

I. INTRODUCTION

Directional orders, such as nematics and ferromagnets, may give rise to topologically nontrivial textures of the order parameter. In ferromagnets, the variety of exchange interactions and host systems translates into a broad spectrum of such textures, such as nonzero Chern numbers in band structures on a kagome lattice [1], merons in coupled disks [2] or multilayers [3], chiral domain walls (DWs) [4–6], and skyrmions [7–9]. Yet, while all those have a continuous spin texture, a singular configuration was theoretically predicted in 1965 [10]: the Bloch point (BP). This is a point defect for the unit magnetization vector field m, and as such the only possible topological defect in ferromagnetism [11]. It is the analog of defects seen in nematic liquid crystals [12,13], for which the distribution of the director around the defect covers the unit sphere $\mathcal{S}^2$ exactly once. For this reason, an integer called winding number [14] is associated to the BP, which is its signature as a topological defect.

The existence of the BP is crucial, as simulation suggested that the transformation from one spin texture to another of different topology is mediated by a BP expulsion or injection: in static [15] or dynamic [16] magnetization switching of vortex cores in thin films, the nucleation of skyrmions in dots [17], or of DWs in magnetically soft cylindrical nanowires [18]. The latter system appears as a textbook playground for the investigation of topological transformations and of BPs. Indeed, BPs should exist at rest, unlike those involved in the dynamical transformation processes mentioned above. In detail, two types of DWs were predicted to exist in cylindrical nanowires, with different topologies. First is the Bloch point domain wall (BPW, also called vortex wall by some), hosting a BP at its center even at rest. The BPW was predicted to reach a steady-state motion with high axial velocity even at high magnetic field [19–21]. Second is the transverse-vortex wall (TVW, also called transverse wall by some), with fast azimuthal precession and axial mobility much lower than that of the BPW [19,22]. Both DWs have been predicted to retain their topology during motion. This makes a sharp contrast with thin strips, prone to DW transformations under both field and spin-polarized current [19,23,24]. The latter can be understood as all DWs share a single topology in strips [25], making transformations easier. As the existence of the BPW and TVW has been confirmed experimentally recently at rest [26,27], the question arises whether the different topology indeed prevents DW transformation in reality.

In this paper, we investigate the field-driven motion of magnetic DWs in magnetically soft nanowires. Our experiments reveal that the transformation from TVW to BPW and vice versa may occur. We build a theoretical understanding of this topological transition, associated with the injection of a BP (or expulsion for the reverse process). Micromagnetic simulations partly confirm this qualitative description, highlighting how the precessional magnetization dynamics leads to the previously overlooked possibility of TVW-to-BPW transformation. However, the BPW-to-TVW transformation is not found in the simulation, leaving open the question whether experiments or models should be blamed.

*alexis.wartelle@wanadoo.fr

†Present address: CEITEC – Central European Institute of Technology, Brno University of Technology, 612 00 Brno, Czech Republic.

‡olivier.fruchart@cea.fr

II. METHODS

Starting from nanoporous alumina templates engineered with two diameter modulations along the pores, we electroplate magnetically soft $Fe_{20}Ni_{80}$ and $Co_{40}Ni_{60}$ nanowires [28–30]. The geometry is thus that of a cylinder with a thin section of diameter ≈140 nm surrounded by two wider sections of the same diameter ≈250 nm, all three with length 10 μm. The purpose of the modulations of diameter is to act as energy barriers around the thin section, thereby confining the DW. After fabrication, the membrane is dissolved in NaOH. After purification of the solution with water and isopropanol, the nanowires are dispersed on a silicon wafer for performing experiments on single objects. DWs are nucleated either upon demagnetization with a high magnetic field perpendicular to the wire axis, or nucleation with pulses of moderate magnetic field applied along the wire axis.

Samples were imaged at synchrotrons Elettra [31] and Alba [32], to monitor DWs with shadow x-ray magnetic circular dichroism coupled to photoemission electron microscopy (XMCD-PEEM). This technique, pioneered by Kimling *et al.* [33], delivers a magnetic contrast map of the projection of magnetization along the beam having gone through the sample. This provides information about magnetization in the wire core [27,29,34] and, combined with simulations of the shadow XMCD contrast [29], allows one to unambiguously determine the DW nature (topology) [27]. In short, BPW patterns are always symmetric with respect to a plane perpendicular to the wire axis, while TVW patterns are not symmetric for the wire diameters considered. In the present experiments, DWs are observed at rest, before and after the application of a quasistatic magnetic field of duration ∼ 1 s, using a dedicated sample holder [35].

Micromagnetic simulations were performed with our homemade finite-elements code FEELLGOOD [36,37], which solves the Landau-Lifshitz-Gilbert equation [38]. Material parameters are those of permalloy: spontaneous induction $\mu_0 M_s$ =1 T, exchange stiffness $A = 10\,\mathrm{pJ/m}$, and no magnetocrystalline anisotropy. This sets the dipolar-exchange length $\sqrt{2A/\mu_0 {M_s}^2}$ at 5 nm, providing the relevant length scaling, to apply the present results to any other soft magnetic material. We used $\alpha = 0.05$ for the damping parameter, and the typical cell size was 2.5 nm. We consider wires of finite length, however, compensate their end charges, so as to mimick infinitely long wires. We name z the direction along the wire axis, and x and y the transverse directions. While remaining in the same order of magnitude, for the sake of computational efficiency we considered smaller diameters in the simulation (70 nm) than in experiments (140 nm). Comparison with existing results suggests that what matters for DW transformation is the consideration of a minimum value of diameter, however, whose precise value we did not determine.

III. EXPERIMENTS

We first recall the features of TVWs and BPWs, whose simulated configurations at rest in a 70-nm-diameter wire are shown in Fig. 1. The former has dual transverse and vortex features [25]. The intercept of the TVW's core (magnetized transverse to the wire axis) with the surface is highlighted

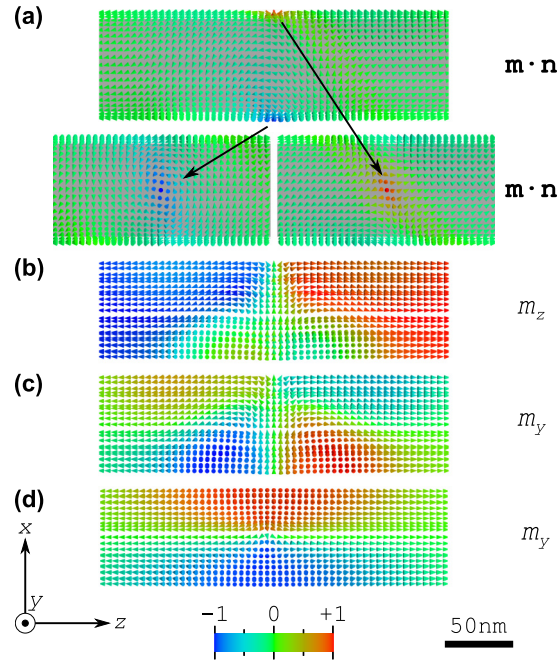

FIG. 1. Simulated tail-to-tail DWs in a 70-nm-diameter wire, magnetization being represented as cones. (a) TVW surface magnetization with color coding m · n, n being the outward normal to the wire surface. The gray background highlights the extent of the wire. The two bottom insets show the same rotated by $\mp\pi/2$, highlighting the vortex and antivortex of the inlet and outlet of transverse magnetization. (b),(c) Slice through the TVW, with m_z and m_y color code. (d) Slice through the BPW, with m_y color code.

by the color map of m · n in Fig. 1(a), where n is the local, outward-pointing normal to the wire surface. The core of the DW is better seen in the cross-sectional view in Fig. 1(b), displaying a triangular shape reminiscent of the transverse wall in soft flat strips. The vortex feature is illustrated by the winding of magnetization around the DW core [Fig. 1(c)]. It has a counterpart on the opposite side (bottom on the figure), which defines an antivortex. In contrast to this, the BPW possesses no core with transverse magnetization [Fig. 1(d)]. It has full symmetry of rotation around the wire axis with a curling of magnetization, and a mirror symmetry perpendicular to the latter. For continuity reasons the BPW must feature a BP singularity at its center.

Figure 2 shows DWs in wires, imaged with PEEM. Only the shadow is visible, not the wire itself, related to the focus settings. The choice of in-plane angle of the beam, close to 70° away from the wire axis, provides magnetic contrast from both the domains and the DWs. A bipolar contrast in the shadow of the DW is the signature of the BPW [29]. This is the case for Figs. 2(a)–2(c) and 2(e). To the contrary, the less symmetric contrast in Fig. 2(d) is indicative of a TVW [29] (see Supplemental Material [39]).

This series of images provides two examples of DW transformation, taken among a larger series. The DW moves reliably between the same pinning sites above a threshold around 10 mT, probably at high speed and then remaining pinned during the remainder of the field pulse: Figures 2(a) and 2(c) are both a starting configuration with a tail-to-tail

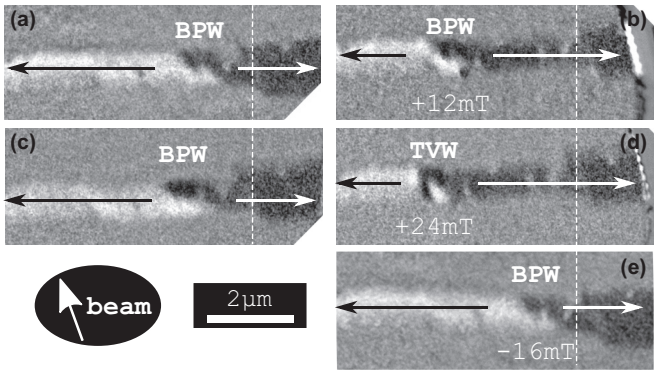

FIG. 2. XMCD-PEEM views under zero magnetic field of the shadow of a 140-nm-diameter $Fe_{20}Ni_{80}$ nanowire, featuring a tail-to-tail DW in its thin section. Arrows stand for magnetization in the domains, and the vertical dotted line indicates the diameter modulation. (a),(b) and (c),(d) are two sequences initialized with a BPW followed by the application of a quasistatic field with strength 12 and 24 mT, respectively, as indicated in the final image. (e) follows (d), after application of −16 mT.

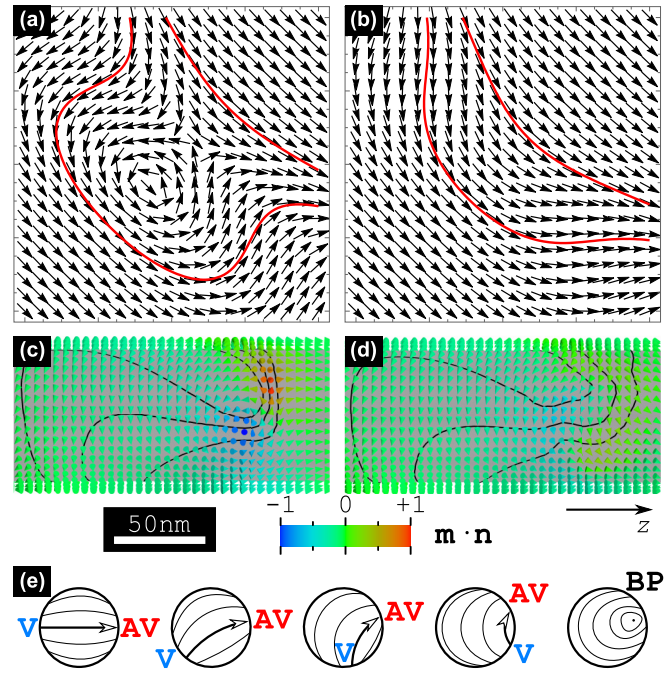

FIG. 3. Top row: unrolled maps of the parametrized vector field a_t before (a) and after (b) the merging of the vortex-antivortex pair. Two field lines are displayed. Bottom: micromagnetic simulation of the transformation of a TVW under a magnetic field $\mu_0 H_a$=8.2 mT, with snapshots at $t_1 = 0.45$ ns and $t_2 = 0.62$ ns $> t_c$, i.e., before and after the transformation process. (e) Illustration of the process of the expulsion of the core of the TVW. V, AV, and BP stand for vortex, antivortex, and Bloch point, respectively.

BPW. The outcome of the application of a magnetic field depends on its strength. Under 12 ± 1 mT the DW is displaced without visible changes to the configuration [Fig. 2(b)]. Under 24 ± 1 mT the DW is displaced and its final topology changed to TVW [27,29] [Fig. 2(d)]. Repeating this experiment for the opposite (i.e., head-to-head; see Supplemental Material) DW polarity led to the same result. Transformations from a TVW to a BPW were also observed, with a similar threshold [Fig. 2(e)]. Finally, we also investigated $Co_{40}Ni_{60}$ as another rather soft magnetic material, for the sake of generality. DWs may also transform from BPW to TVW and vice versa, with a threshold field of 9 mT, proving that the phenomenon is not limited to a specific sample or material (Supplemental Material Fig. 3).

IV. THEORETICAL DESCRIPTION AND DISCUSSION

These experiments show that the injection or annihilation of the micromagnetic BP topological defect is possible, and does not require extremely high field. In other words, the distinct topological natures of the BPW and the TVW do not prevent these DWs from transforming into one another. However, the transformation process, of precessional nature [16], cannot be grasped by static imaging. Therefore, we first turn to a parametric description to understand the path followed during the transformation, which is a usual tool to describe bifurcations and symmetry breaking. We define a unit vector field a_t standing for magnetization at the surface of a cylinder. a_t is defined from the unit vector orthogonal to the gradient of a third-order polynomial defined on a planar surface, and is thus always tangent to the cylinder (see Supplemental Material). It is chosen in such a way that it features the aforementioned vortex-antivortex pair, and respects the boundary conditions with domains of opposite orientation at both ends. One of the polynomial's coefficients is parametrized with a pseudotime τ. At $\tau = 0$, the polynomial has a local minimum corresponding to the vortex, and a saddle point corresponding to the antivortex. As τ increases, the polynomial's local minimum and saddle point are brought closer [Figs. 3(a) and 3(b)], until they merge at a critical time $\tau_c < 1$ into an inflexion point. Later on, for $\tau_c < \tau < 1$, the polynomial no longer has any extremum or inflexion point [Fig. 3(b)]. The time line could be reversed to equally describe the transformation of a BPW into a TVW.

It can be checked that the $\mathcal{S}^2$ winding number associated to the parametric vector field is such that $N_p(\tau < \tau_c) = 0$, while $N_p(\tau > \tau_c) = 1$. This indicates that any normalized continuation of a_t into the cylinder's interior *must* contain a singular point. Thus, the vortex-antivortex pair is annihilated on the wire surface at $\tau_c < 1$, and associated with the injection of a BP into the volume [Fig. 3(e)].

The physical validity of the mechanism described above must be checked with micromagnetic simulations. To that end, we start from a tail-to-tail TVW configuration in a 70-nm-diameter and 1-μm-long FeNi wire relaxed under zero magnetic field. We then apply a constant field in a stepwise manner at $t = 0$. We evidence the existence of a threshold field in the simulations, consistent with the experiments. In the low-field regime the DW precesses around the wire axis while slowly moving forward, soon reaching a steady-state regime in a rotating frame. This is consistent with prior knowledge about TVWs [19,40,41]. We detail below the high-field regime, with the selected case $H = 8.2$ mT slightly above the threshold. After $t_1 = 0.45$ ns the vortex and antivortex are no longer diametrically opposed but rather close to one another,

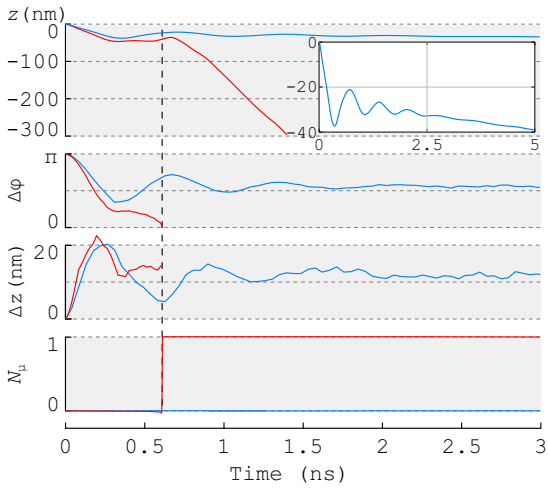

FIG. 4. Numerical micromagnetic indicators versus time for DW motion below (blue, 6 mT) and above (red, 8.2 mT) the threshold field H_c: position z, azimuthal and axial separation of vortex versus antivortex $\Delta\varphi$ and Δz, and winding number N_μ. The vertical line indicates the time of change of topology.

as shown by the neighboring extrema of opposite signs in the color map of $\mathrm{m}\cdot\mathrm{n}$ [Fig. 3(c)]. This dynamical effect is not surprising, as two aspects break the symmetry between the vortex and antivortex: (1) owing to the triangular shape of the TVW [Figs. 1(b) and 1(c)], the surface wall width is different on opposite sides. Thus, if one applies handwavingly the one-dimensional model to surface magnetization, a given torque arising from the applied field translates into different velocities. (2) The gyrovectors of the vortex and antivortex differ, contributing to a difference in both the longitudinal and azimuthal motion. We write N_μ the winding number in the simulations. While $N_\mu(t_1) \approx 0$, consistent with the parametric model, the calculated surface isolines of $m_z = -0.8$, 0, and 0.8 are quite pinched. At $t_2 = 0.62$ ns, these curves have become more separated and smooth, and visually the vortex and antivortex have both disappeared [Fig. 3(d)]. This suggests the injection of a Bloch point resulting from the recombination into the volume of the vortex-antivortex annihilation at the surface, which is formally confirmed as $N_\mu(t_2) \approx 1$. Another view is the following: the line of magnetization linking the surface vortex and antivortex through the wire, initially the straight transverse component, becomes an arc getting shorter over time, until being completely expelled from the wire at t_c [Fig. 3(e)].

We can monitor the transformation quantitatively with numerical indicators (Fig. 4). First, $N_\mu(t)$ shows an abrupt jump consistent with the nucleation of a BP and the change of topology, from which we determine the critical time $t_c \approx 0.61$ ns. Second, we monitor the positions of the vortex and antivortex, from the extrema of $\mathrm{m}\cdot\mathrm{n}$. We then compute the difference in angular position $\Delta\varphi(t) = \varphi_{\mathrm{AV}}(t) - \varphi_{\mathrm{V}}(t)$ and in the abscissa along the wire axis $\Delta z(t) = z_{\mathrm{AV}}(t) - z_{\mathrm{V}}(t)$. Starting from $\Delta\varphi(0) = \pi$ and $\Delta z(0) = 0$, $\Delta\varphi$ decreases monotonuously, while $\Delta z(t)$ first increases before decreasing again. Ultimately, both quantities become undefined at t_c. Note that the DW velocity sharply increases after the transformation [see $z(t)$], in agreement with existing knowledge regarding BPWs versus TVWs [19,42]. Figure 4 also shows the time evolution of those numbers below the field threshold for the transformation. The initial trend is similar, the vortex moving faster than the antivortex axially, and rotating slower. However, $\Delta\varphi$ and Δ_z eventually reach a plateau instead of vanishing. The reason is that the field-driven torque is too weak to overcome the cost in exchange when the vortex and antivortex draw nearer. This also probably explains why the DW transformation in wires of constant diameter had been overlooked in simulations so far: significantly smaller diameters were considered, associated with a larger exchange cost to bend the DW core and join vortex and antivortex, preventing the transformation. Overall, experiments and theory agree on the existence of a threshold field for the TVW-to-BPW transformation, with value around 10 mT. The quantitative agreement is surprisingly good, given the possible interplay of material imperfections in experiments, and the difficulty to accurately describe sharply varying magnetization textures and BPs in micromagnetics [15,43–45].

To the contrary, while we witness the reverse process in the experiments (BPW to TVW), again with the existence of a threshold (however, with typically 50% higher value), this is not reproduced by simulation, up to at least 50 mT. At low applied field, at least up to 20 mT, a steady-state motion of the BPW occurs, with perfect azimuthal rotational symmetry. At larger fields, the BPW emits droplets from its back tail, comprising an anti-Bloch point and a Bloch point. These quickly annihilate, creating spin waves. This change of regime at high magnetic field was already reported [42]. It can be explained handwavingly from the one-dimensional model [19] by the lower field-driven local mobility of the Bloch point compared with the periphery of the BPW, due to its smaller length scale. However, in both regimes the Bloch point remains essentially close to the wire axis, preserving the topology of the BPW. At this point, it remains an open question whether it is imperfections in the experiments or lacking ingredients in theory, which are to be blamed. Experimental imperfections could consist of grains and grain boundaries, creating a local energy landscape for the BP. Through breaking the rotational symmetry, this energy landscape could induce enough radial momentum to the Bloch point to drive it toward the wire surface. Note that, although the simulated motion of the BPW is rather stable, numerical imperfections also exist. For example, the interaction with the underlying discretization cells, which even in atomistic models gives rise to a local landscape of energy [20]. This interaction with the underlying numerical lattice could be the reason for numerical instabilities, such as the helical motion of the BP reported at high applied field [21].

V. CONCLUSION

We observed experimentally the topological transformation of domain walls in cylindrical nanowires upon motion under magnetic field, from the transverse-vortex type (TVW) to the Bloch-point type (BPW) and the reverse, with a threshold in the range of 10 mT. Our micromagnetic simulations confirm the possibility for some wall transformation, namely, from TVW to BPW, involving the nucleation of a Bloch point at the wire surface. This is a turning point in the topic, as

not only is this an experimental report of DW structure upon motion following 15 years of numerous theoretical reports, but it points at the possibility of wall transformation previously overlooked because of the consideration of too small diameters. This calls for the reexamination of the unique features predicted previously, such as absence of breakdown field [19,20] and the spin-Cherenkov effect [46]. This also calls for further experimental work, such as time-resolved imaging to compare the process to simulations, and material science work to understand to what extent pinning and defects may play a role.

ACKNOWLEDGMENTS

This project has received funding from the European Union Seventh Framework Programme (FP7/2007-2013) under Grant Agreement No. 309589 (M3d). M.S. acknowledges a grant from the Laboratoire d'Excellence LANEF in Grenoble (Grant No. ANR-10-LABX-51-01). The PEEM experiments performed at ALBA Synchrotron involve the collaboration of ALBA staff, with special thanks to Jordi Prat. We thank Benjamin Canals from Institut Néel and Michel Hehn from Institut Jean Lamour for fruitful discussions.

[1] M. Taillefumier, B. Canals, C. Lacroix, V. K. Dugaev, and P. Bruno, Phys. Rev. B **74**, 085105 (2006).

[2] C. Phatak, A. K. Petford-Long, and O. Heinonen, Phys. Rev. Lett. **108**, 067205 (2012).

[3] A. Hierro-Rodriguez, C. Quirós, A. Sorrentino, C. Blanco-Roldán, L. M. Alvarez-Prado, J. I. Martín, J. M. Alameda, E. Pereiro, M. Vélez, and S. Ferrer, Phys. Rev. B **95**, 014430 (2017).

[4] G. Chen, A. T. N'Diaye, S. P. Kang, H. Y. Kwon, C. Won, Y. Wu, Z. Q. Qiu, and A. K. Schmid, Nat. Commun. **6**, 6598 (2015).

[5] J.-P. Tetienne, T. Hingant, L. Martinez, S. Rohart, A. Thiaville, L. H. Diez, K. Garcia, J.-P. Adam, J.-V. Kim, J.-F. Roch, I. M. Miron, G. Gaudin, L. Vila, B. Ocker, D. Ravelosona, and V. Jacques, Nat. Commun. **6**, 6733 (2015).

[6] G. Chen and A. K. Schmid, Adv. Mater. **27**, 5738 (2015).

[7] C. Moreau-Luchaire, C. Moutafis, N. Reyren, J. Sampaio, C. A. F. Vaz, N. V. Horne, K. Bouzehouane, K. Garcia, C. Deranlot, P. Warnicke, P. Wohlhüter, J. M. George, M. Weigand, J. Raabe, V. Cros, and A. Fert, Nat. Nanotechnol. **11**, 444 (2016).

[8] S. Heinze, K. von Bergmann, M. Menzel, J. Brede, A. Kubetzka, R. Wiesendanger, G. Bihlmayer, and S. Blügel, Nat. Phys. **7**, 713 (2011).

[9] O. Boulle, J. Vogel, H. Yang, S. Pizzini, D. de Souza Chaves, A. Locatelli, T. O. Menteş, A. Sala, L. D. Buda-Prejbeanu, O. Klein, M. Belmeguenai, Y. Roussigné, A. Stashkevich, S. M. Chérif, L. Aballe, M. Foerster, M. Chshiev, S. Auffret, I. M. Miron, and G. Gaudin, Nat. Nanotechnol. **11**, 449 (2016).

[10] R. Feldtkeller, Z. Angew. Phys. **19**, 530 (1965).

[11] H. B. Braun, Adv. Phys. **61**, 1 (2012).

[12] C. Williams, P. Pieranski, and P. E. Cladis, Phys. Rev. Lett. **29**, 90 (1972).

[13] A. Saupe, Mol. Cryst. Liq. Cryst. **21**, 211 (1973).

[14] J. H. C. Whitehead, Proc. Natl. Acad. Sci USA **33**, 117 (1947).

[15] A. Thiaville, J. M. Garcìa, R. Dittrich, J. Miltat, and T. Schrefl, Phys. Rev. B **67**, 094410 (2003).

[16] B. Van Waeyenberge, A. Puzic, H. Stoll, K. W. Chou, T. Tyliszczak, R. Hertel, M. Fähnle, H. Brückl, K. Rott, G. Reiss, I. Neudecker, D. Weiss, C. H. Back, and G. Schütz, Nature (London) **444**, 461 (2006).

[17] J. Sampaio, V. Cros, S. Rohart, A. Thiaville, and A. Fert, Nat. Nanotechnol. **8**, 839 (2013).

[18] R. Hertel, J. Magn. Magn. Mater. **249**, 251 (2002).

[19] A. Thiaville and Y. Nakatani, in *Spin Dynamics in Confined Magnetic Structures III*, Topics in Applied Physics, Vol. 101, edited by B. Hillebrands and A. Thiaville (Springer, Berlin, Heidelberg, 2006), pp. 161–206.

[20] R. Hertel and C. Andreas, in *Magnetic Nano- and Microwires* (Woodhead, Cambridge, UK, 2015), p. 653.

[21] R. Hertel, J. Phys.: Condens. Matter **28**, 483002 (2016).

[22] M. Yan, A. Kákay, S. Gliga, and R. Hertel, Phys. Rev. Lett. **104**, 057201 (2010).

[23] G. S. D. Beach, C. Nistor, C. Knuston, M. Tsoi, and J. L. Erskine, Nat. Mater. **4**, 741 (2005).

[24] A. Thiaville and Y. Nakatani, in *Nanomagnetism and Spintronics*, edited by T. Shinjo (Elsevier, New York, 2009), Chap. 6, pp. 231–276.

[25] S. Jamet, N. Rougemaille, J. C. Toussaint, and O. Fruchart, in *Magnetic Nano- and Microwires: Design, Synthesis, Properties and Applications*, edited by M. Vázquez (Woodhead, Cambridge, UK, 2015), pp. 783–811.

[26] N. Biziere, C. Gatel, R. Lassalle-Balier, M. C. Clochard, J. E. Wegrowe, and E. Snoeck, Nano Lett. **13**, 2053 (2013).

[27] S. Da Col, S. Jamet, N. Rougemaille, A. Locatelli, T. O. Mentes, B. S. Burgos, R. Afid, M. Darques, L. Cagnon, J. C. Toussaint, and O. Fruchart, Phys. Rev. B **89**, 180405 (2014).

[28] S. Da Col, S. Jamet, M. Staňo, B. Trapp, S. L. Denmat, L. Cagnon, J. C. Toussaint, and O. Fruchart, Appl. Phys. Lett. **109**, 062406 (2016).

[29] S. Jamet, S. Da Col, N. Rougemaille, A. Wartelle, A. Locatelli, T. O. Menteş, B. Santos Burgos, R. Afid, L. Cagnon, S. Bochmann, J. Bachmann, O. Fruchart, and J. C. Toussaint, Phys. Rev. B **92**, 144428 (2015).

[30] A. Wartelle, C. Thirion, R. Afid, S. Jamet, S. Da Col, L. Cagnon, J.-C. Toussaint, J. Bachmann, S. Bochmann, A. Locatelli, T. Onur Mentes, and O. Fruchart, IEEE Trans. Magn. **51**, 4300403 (2015).

[31] A. Locatelli, L. Aballe, T. O. Menteş, M. Kiskinova, and E. Bauer, Surf. Interface Anal. **38**, 12 (2006).

[32] L. Aballe, M. Foerster, E. Pellegrin, J. Nicolas, and S. Ferrer, J. Synchrotron. Radiat. **22**, 745 (2015).

[33] J. Kimling, F. Kronast, S. Martens, T. Böhnert, M. Martens, J. Herrero-Albillos, L. Tati-Bismaths, U. Merkt, K. Nielsch, and G. Meier, Phys. Rev. B **84**, 174406 (2011).

[34] R. Streubel, L. Han, F. Kronast, A. A. Unal, O. G. Schmidt, and D. Makarov, Nano Lett. **14**, 3981 (2014).

[35] M. Foerster, J. Prat, V. Massana, N. Gonzalez, A. Fontsere, B. Molas, O. Matilla, E. Pellegrin, and L. Aballe, Ultramicroscopy **171**, 63 (2016).
[36] F. Alouges, E. Kritsikis, J. Steiner, and J.-C. Toussaint, Numer. Math. **128**, 407 (2014).
[37] See http://feellgood.neel.cnrs.fr.
[38] T. Gilbert, IEEE Trans. Magn. **40**, 3443 (2004).
[39] See Supplemental Material at http://link.aps.org/supplemental/10.1103/PhysRevB.99.024433 for technical information concerning the microscopy images, data with larger statistics, and mathematical details for the modeling.
[40] R. Hertel, J. Appl. Phys. **90**, 5752 (2001).
[41] H. Forster, T. Schrefl, D. Suess, W. Scholz, V. Tsiantos, R. Dittrich, and J. Fidler, J. Appl. Phys. **91**, 6914 (2002).
[42] R. Hertel and J. Kirschner, J. Magn. Magn. Mater. **278**, L291 (2004).
[43] R. G. Elías and A. Verga, Eur. Phys. J. B **82**, 159 (2011).
[44] K. M. Lebecki, D. Hinzke, U. Nowak, and O. Chubykalo-Fesenko, Phys. Rev. B **86**, 094409 (2012).
[45] R. Hertel and A. Kakay, J. Magn. Magn. Mater. **369**, 189 (2014).
[46] M. Yan, C. Andreas, A. Kakay, F. Garcia-Sanchez, and R. Hertel, Appl. Phys. Lett. **99**, 122505 (2011).